

JLAB12 Activity report 2018

V. Lucherini, M. Mirazita (Resp.), D. Orecchini(Tecn.), A. Orlandi(Tecn.),
P. Rossi, O. Soto (INFN fellowship), S. Tomassini, M. Turisini (Ass.), A. Viticchie' (Tecn.)

1 Introduction

The JLAB12 group of LNF participates in the physics program carried on by the CLAS collaboration in the Hall B of the Jefferson Laboratory (JLab). The CLAS experiment in 2018 restarted the physics activity after a long break due to the upgrade of the Laboratory. The LNF group has been deeply involved in the commissioning of the CLAS12 detector, in the data taking and in the first analyses of the physics data. In parallel, the construction of the second RICH module has been started.

2 The CLAS12 RICH

The Ring Imaging Cherenkov (RICH) detector has been built to provide the CLAS12 spectrometer with the capability to distinguish kaons from pions and protons in the momentum range between 3 and 8 GeV/c. The detector is composed by an aerogel radiator, an array of multianode photomultiplier tubes (MAPMTs) for the Cherenkov light detection and a mirror system. All these elements are contained in a large trapezoidal box, of approximate height of 3.5 m and large base of about 4 m. The radiator is composed by tiles with squared shape 20×20 cm² as well as smaller pentagonal, trapezoidal or triangular tiles to fit the detector shape. The total number of tiles is 102, assembled in two sections: the forward angle one made by one layer with 2 cm thickness and the large angle one made by two layers with 3 cm thickness each. The mirror system is composed by 10 carbon fiber spherical mirrors and 10 glass planar mirrors, for a total surface of about 10 m². The goal of the mirror system is to contain as much of the produced Cherenkov inside the detector and to direct them toward the photodetector array. The photodetector array uses 391 MAPMT Hamamatsu H8500 and H12700. These two types of tubes are composed by a matrix of 8×8 matrix of pixel with about 6 mm pixel size, with a total of 25024 independent readout channels.

The readout electronics is based on the MAROC3 chip, a 64 channel microcircuit dedicated to MAPMT pulse processing. Each channel offers a low impedance adjustable gain preamplifier followed by a highly configurable shaping section, and produces prompt logic pulses from an adjustable threshold discriminator. The MAROC is configured and read out by a FPGA optically linked with the data acquisition node. The front-end electronics is organized in compact units mechanically designed to fit the MAPMT dimensions and serving two or three MAPMTs each, thus allowing the tessellation of large surfaces with minimum dead space and material budget.

The assembly of the detector was completed by the mid of December 2017 and was installed in CLAS12 in January 2018.

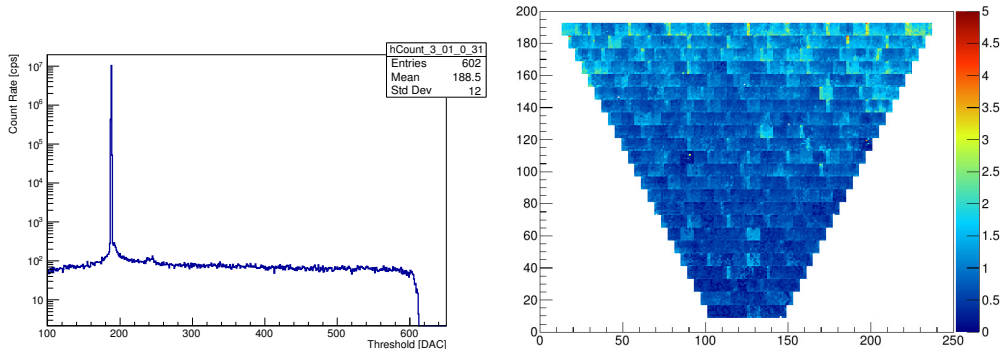


Figure 1: Typical dark noise spectrum as a function of the readout discriminator threshold (left plot) and distribution of the RMS of the pedestals (right plot).

2.1 The RICH Commissioning

The Commissioning of the RICH detector has been started during the assembly phase and has been completed after its installation in CLAS12 in January 2018.

The characterization measurements on the MAPMTs and the readout electronics performed before the assembly provided position and resolution of the single photon (*spe*) spectrum. Channel-by-channel variation of the gains of the order of 1 to 3 have been found, in agreement with the expectations based on the datasheets from the Hamamatsu, and compensated by appropriately choosing the individual preamplifier gains.

The basic performance and the stability of the readout electronics were verified by performing dark noise measurements using the scaler readout. The main parameters measured, channel by channel and averaged per PMT, are the pedestal width and position (with PMT high voltage off or on), the dark noise count rate as a function of the discriminator threshold. An example of the dark noise spectrum for one channel is shown in the left plot of Fig. 1. We see a very narrow pedestal peak (few mV) and an almost flat single photon spectrum as the threshold increases. The distribution of the RMS of the pedestals is shown in the right plot of Fig. 1. Very few channels have RMS larger than few threshold units. Typical measured dark noise rate values are below 100 Hz for more than 99% of the total readout channels, and less than 10 channels were found with dark rate above 10 kHz. Dark noise measurements have been periodically repeated and no major variations in the response have been found.

The first weeks of data taking after the installation have been dedicated to several tests to verify the functioning of the detector with the electron beam. Data have been taken by varying the beam current, with different intensity of the toroidal and solenoidal fields, including zero field for alignment studies, with full and empty target, etc.. As an example, in Fig. 2 we show the average count rate for the MAPMT 3 and 5 measured with the scaler readout as a function of the electron beam current. We found a linear response over the whole explored beam current interval and up to about 120 nA, as indicated by the fit with a linear curve reported on the plot. The current during the regular data taking is usually comprised between 40 and 70 nA. The intercept of the linear curve provided the count rate at zero beam current, i.e. the dark count rate. The values obtained in this way have been found reasonably in agreement with the measurements without the beam already discussed in this section.

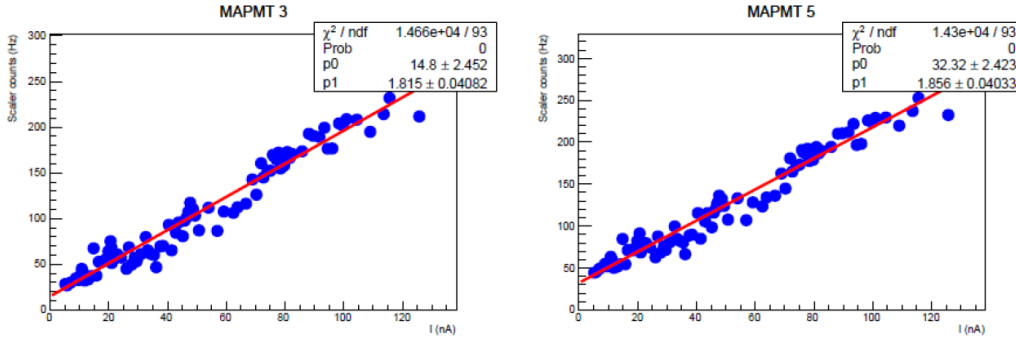


Figure 2: Average count rate measured on two MAPMTs as a function of the beam current.

2.2 Performance of the RICH detector: time calibration

For each event and for a given channel, the RICH readout provides a number of edge times, i.e. the times at which the input signal crossed the discriminator threshold. A hit is reconstructed by pairing a leading and a trailing edge in the correct temporal sequence. The leading edge then provides the time of the hit, while the difference between the trailing and the leading edge, i.e. the duration of the hit, is roughly proportional to the amplitude of the input signal. The time calibration is performed by computing the difference ΔT between the time provided by the RICH and the one calculated by taking into account the CLAS12 event start time, the time for the charged track to reach the aerogel radiator and for the produced photon to reach the MAPMT array. It is assumed in the calculation that the photons are detected directly without any reflection on the mirror system.

In Fig. 3 we show an example of ΔT vs duration plot measured for two different readout channel of MAPMT 55. These plots are equivalent to the well known time walk plots for a system equipped with ADC and TDC readout. The main features of the plots are:

- hits with the shorter time (i.e. smaller amplitude) arrives later in time;
- most of the hits have duration values comprised between 50 and 60 ns: this is the *spe* region;
- the curve extends to smaller duration: this is the cross talk region;
- in the *spe* region the dependence of the time from the duration is very weak and the slope of the curve is close to zero; a larger slope is found in the time walk region;
- the fraction of background hits out of the signal band are very scarce;
- the arrival time of the *spe* hits differs from pixel to pixel;
- the shape of the ΔT vs duration curve of the two pixel is very similar.

These considerations have been confirmed also after a detailed channel-by-channel study of the RICH response. Therefore, the following time calibration procedure has been established. We first calculate a set of 25024 time offset constants, one per readout channel, that bring the ΔT of the *spe* hits centered to zero. Then, we calculate a time walk correction function for each PMT. In the current implementation, this curve is made by the combination of two straight lines, the first one representing the *spe* region and the second one to reproduce the cross talk region. The two lines join at a value ΔT_0 representing the boundary between the *spe* and the cross talk region.

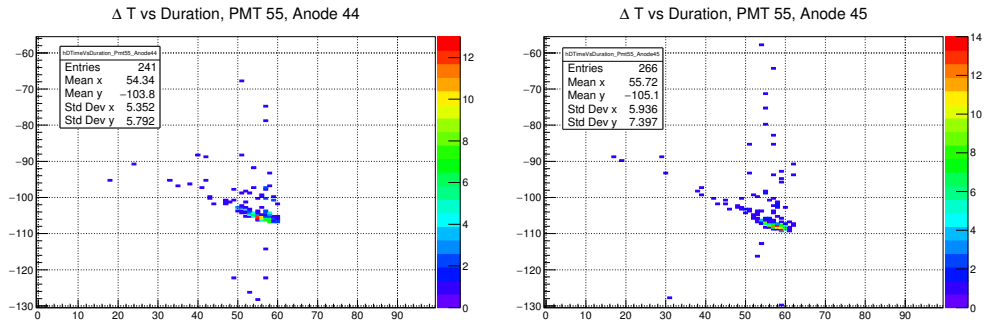


Figure 3: Curve of the measured ΔT as a function of the duration for channel 44 and 45 of MAPMT 55.

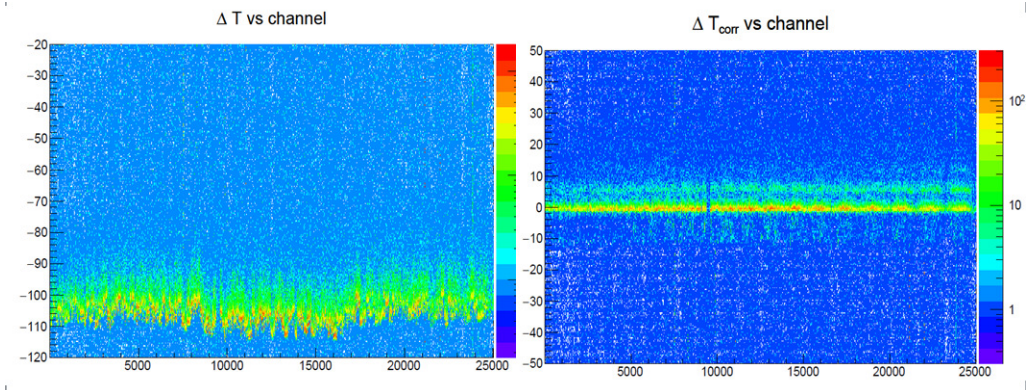


Figure 4: Distributions of the ΔT of all the readout channels before (left plot) and after (right plot) the application of the time calibration procedure.

This simple parametrization has been chosen as a compromise between flexibility in reproducing the data and robustness in order to minimize the number of failed fits.

The effectiveness of the procedure is demonstrated in Fig. 4, where we show the ΔT distributions of all the channels before (left plot) and after (right plot) the calibration procedure has been applied. All the channels have the main peak centered at zero and the weaker bands we see in the plot are produced by reflected photons or out of time tracks.

The final time resolution we achieved is of the order of $\sigma_T \approx 0.7$ ns, well below the required 1 ns necessary to distinguish reflected photons from those detected directly after the emission.

2.3 Performance of the RICH detector: Cherenkov angle reconstruction

The complicated geometry of the RICH requires a sophisticated reconstruction algorithm that takes into account all the possible hit pattern distributions, considering that in general events will mix together direct and reflected photons. Knowing the charged tracks passed through the aerogel radiator, the RICH event reconstruction software will provide a set of likelihood values for all the possible mass hypothesis associated to each track. This algorithm is currently under development.

We present here the preliminary results of a simplified version applied to events with one single electron detected in the RICH. This simplified version utilizes the analytic solution already

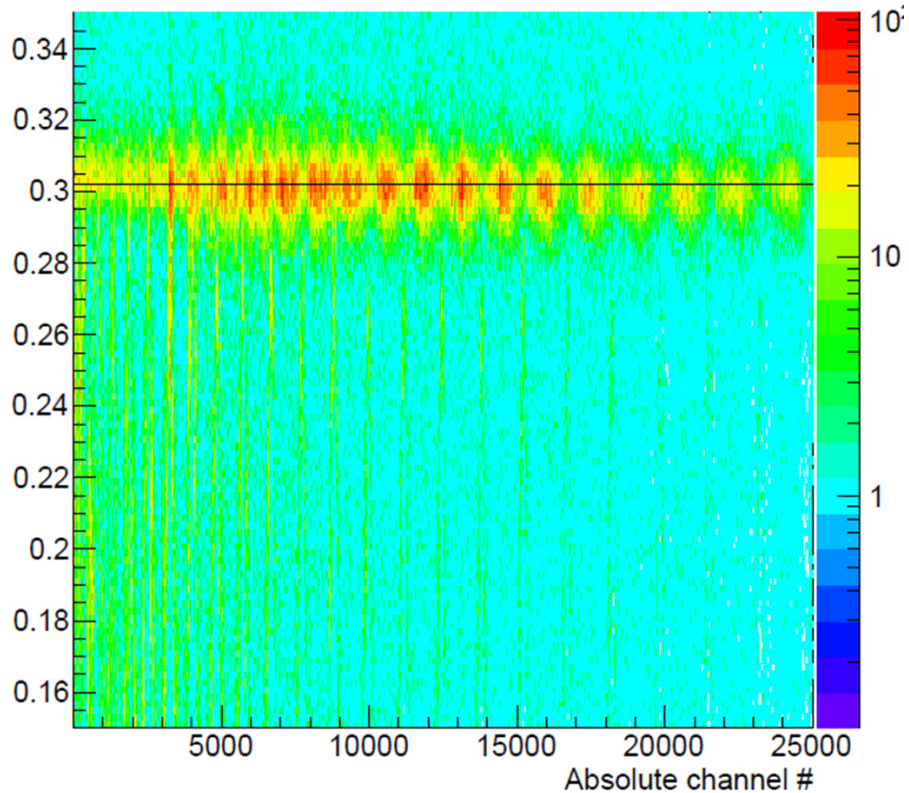


Figure 5: *Cherenkov angle distribution (in mrad) as a function of the readout channel. The black lines indicates the expected Cherenkov angle for electron on a radiator with refractive index $n=1.049$.*

applied in the reconstruction of the CERN test beam of the RICH prototype ¹⁾ and valid only for photons detected without any reflection.

We first select electrons by using the tracking information together with the High Threshold Cherenkov Counter and the calorimeters of the CLAS12 spectrometer. A cut on the momenta below 1.5 GeV/c is applied to avoid Cherenkov angle variations due to the lower electron velocity.

If one electron passes through the glass window of the MAPMTs, it typically produces a cluster of hits with high multiplicity on one single MAPMT. Those hits are labelled and removed from the Cherenkov angle reconstruction process. For the remaining Cherenkov photon hit candidate, the time calibration correction is applied and on time photons are selected by applying a 3σ in the ΔT distributions shown in the right plot of Fig. 4. For these hits, the Cherenkov angle is computed.

The distribution of the reconstructed Cherenkov angles as a function of the readout channel are shown in Fig. 5. We see a clear signal on all the channels. The distribution of the intensity of the signal reflects the production rate combined with the acceptance for direct detection. The line reported on the plot indicates the expected Cherenkov angle for electron passing through an aerogel radiator with refractive index $n=1.049$, the average value for the tiles we used.

2.4 Construction of the second RICH module

The installation of a second RICH module is planned, allowing to double the charged kaon acceptance of the CLAS12 spectrometer and also to better control the systematics uncertainties in the future measurements with a transversely polarized target.

The construction of the second module, with the same geometry of the first one, is currently underway under the supervision of the physicists, technologists and technicians of the LNF group. The construction of the mechanical structure of the detector has been awarded in 2018 to the *Tecnologie Avanzate srl* company, the same that built the first module, and will begin in 2019. The purchase of the internal components has also started. We expect the delivery of the aerogel of the first 3 cm layer and of the MAROC3 chips by the first quarter of 2019.

3 The CLAS physics data taking and analysis

The physics data taking of the CLAS experiment has started in February 2018. The first run, from February to May, was dedicated to the so called *Run Group A*, that includes 13 different experiments and utilized a 10.6 GeV energy electron beam with polarization greater than 80% and an unpolarized liquid hydrogen target. After the summer break, the data taking was resumed and included also the *Run Group K* (3 experiments with lower energy electron beam and unpolarized hydrogen target) and *Run Group B* (7 experiments with 10.6 GeV electron beam and unpolarized liquid deuterium target). All these experiments, five of them with members of the LNF group as spokesperson, are studying various aspects of the hadronic physics by looking at exclusive as well as inclusive or semi-inclusive final states.

A small sample of the *Run Group A*, corresponding to few days of data taking, was made quickly available for the first analysis. Many parallel studies have been performed on these data, to verify the performance of the detector and to check its ability to reproduce existing measurements. In september 2018 the CLAS Collaboration released the first preliminary physics results and were presented for the first time at the SPIN 2018 Conference in Ferrara by a member of the LNF group ³⁾. As an example of the results presented, we show in Fig. 6 the azimuthal angle ϕ dependence of the raw Single Beam Spin Asymmetry measured in the Semi-Inclusive electroproduction of π^+ in the Deep Inelastic region (SIDIS). The plot show a clear $\sin \phi$ modulation, as also indicated by the fit performed on the data.

One of the analysis currently underway which is under the responsibility of members of the LNF group is the study of the SIDIS electroproduction of pion pairs. The advantage of this channel relies in the fact that the Fourier components of the production cross section can be written as simple product of Parton Distribution Functions (PDFs) and Di-Hadron Fragmentation Functions (FFs). This makes their extraction from the experimental data easier with respect to the usual single hadron electroproduction, where instead PDFs and single hadron FFs appear in convolution integrals.

This analysis is just started on the data collected during the first *Run Group A* run (hydrogen target) and will be soon extended to the *Run Group B* run (deuterium target). We show in the left plot of the Fig. 7 the kinematic coverage Q^2 vs Bjorken- x for the $ep \rightarrow e\pi^+\pi^-X$ final state and in the right plot of that figure the distribution of the invariant mass of the two pion pair. These plots have been done utilizing a statistics corresponding to few hours of data taking.

4 Publications

Publications on the RICH activity besides the CLAS Collaboration.

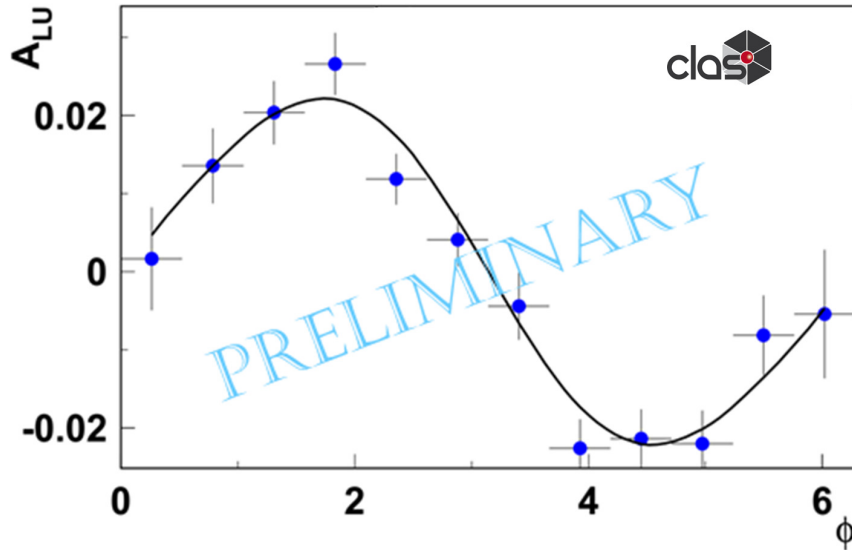


Figure 6: Raw Beam Spin Asymmetry in the SIDIS electroproduction of π^+ . The curve is a fit to the data with a $\sin \phi$ function.

1. M. Mirazita, “The Large-area Hybrid-optics CLAS12 RICH: assembling, commissioning and first data taking”, Proceeding of the RICH 2018 Conference (July 29 - August 4 2018, Moscow - Russia), submitted to Nucl. Inst. Meth..
2. M. Mirazita for the CLAS Collaboration, “First CLAS12 results in SIDIS measurements”, Proceeding of the SPIN 2018 Conference (September 10-14 2018, Ferrara - Italy), submitted to Proceedings of Science.

References

1. S. Anefalo Pereira *et al*, Eur. Phys. J. **A 52**, 23 (2016).
2. S. Blin *et al*, MAROC3 datasheet, October 2010, OMEGA website: <http://omega.in2p3.fr>
3. M. Mirazita “First CLAS12 results in SIDIS measurements”, SPIN 2018 Conference, September 10-14 2018, Ferrara - Italy

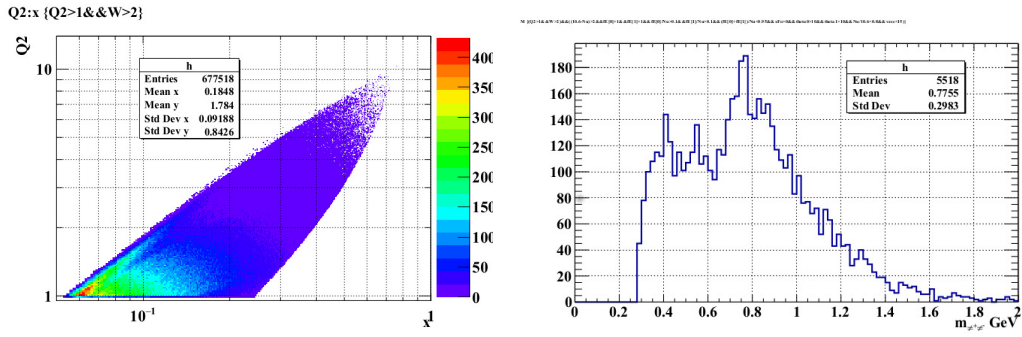


Figure 7: Two pion SIDIS electroproduction: Q^2 vs x_B distribution (left plot) and two pion invariant mass distribution (right plot).